Light-modulated 0-π transition in a silicene-based Josephson junction

Xingfei Zhou and Guojun Jin[*]

National Laboratory of Solid State Microstructures, Department of Physics, and Collaborative Innovation Center of Advanced Microstructures, Nanjing University, Nanjing 210093, China

We investigate the Andreev bound states (ABSs) and Josephson current in a silicene-based superconductor-normal-superconductor junction modulated by a perpendicular electric field and an off-resonant circularly polarized light. Based on the Dirac–Bogoliubov–de Gennes equation, we analytically derive the ABS levels and show they have different phase-difference dependences, which will remarkably influence the velocity of Cooper pairs and then the Josephson current. In the pristine or gated silicene, the ABS levels always show negative slope, which means that the Josephson current is irreversible because of the time-reversal symmetry. When an off-resonant circularly polarized light is applied, whether or not there is a perpendicular electric field, the ABS levels will have positive slope, leading to the emergence of reversed Josephson current due to the nonzero center-of-mass wave vector of Cooper pairs. In this light-modulated silicene-based Josephson junction, valley polarization provides an alternative mechanism for 0-π transition, very different from that for the conventional ferromagnetic Josephson junctions where the spin polarization is essential.

I. INTRODUCTION

Silicene, the counterpart of graphene, has received much attention due to its topological behavior from the strong spin-orbit coupling and gate-controlled band gap [1–3]. More importantly, silicene-based devices, which can grow on some substrates such as Ag(111) and ZrB$_2$ [4,5], are compatible with conventional silicon-based technology. Its unique properties in electronics, thermoelectrics, optoelectronics, and magnetics have been investigated widely [6–12]. Especially, owing to its available spin and valley degrees of freedom, silicene has sparked huge research interest in spintronics and valleytronics [13–15].

However, in contrast to many works on graphene-based superconducting junctions [16–20], including the Andreev reflection and Josephson effect, the silicene-based superconducting junctions have been studied less [21]. Therefore, the intrinsic properties and possible applications of the silicene-based superconducting junctions deserve to be studied in both theory and experiment. Traditionally, a dc Josephson current is a supercurrent carried by Cooper pairs which tunnel between two superconductors with different macroscopic phases, separated by a thin insulating barrier [22]. When the insulating barrier is replaced by a conductor, the Andreev bound states will exist in the middle region, which come from the round-trip Andreev reflection of the electron and hole with subgap energies between the two superconductors [23,24]. If the middle region is a ferromagnetic metal, i.e., in a superconductor-ferromagnet-superconductor (SFS) junction, the direction of the supercurrent can be reversed [25], as first predicted by Buzdin *et al.* [26] and later reviewed by Buzdin [27]. Here the spin degree of freedom plays a vital role in this well-known 0-π transition.

In silicene, there exist both spin and valley degrees of freedom. Naturally, a simple analogy can be proposed that the valley degree of freedom may play the same role as the spin degree of freedom in the phenomenon of the 0-π transition. The pioneering work on the Andreev reflection and Josephson effect in silicene-based superconducting junctions showed that a Cooper pair is composed of one electron with up (down) spin in the K valley and another electron with down (up) spin in the K' valley [21], but it did not highlight the role of spin as well as the valley degree of freedom in the superconducting transport. In addition, the recent research on valleytronics focuses on searching for the valley polarized current [28] but does not make use of the advantage of the valley degree of freedom adequately. In order to explore more possible applications of the silicene-based superconducting junctions and deepen the role of the valley degree of freedom, we would like to search for the valley-related 0-π transition, analogous to the one related to the spin degree of freedom.

In this work, we investigate the Andreev bound states and Josephson current in a silicene-based superconductor-normal-superconductor (SNS) junction, schematically shown in Fig. 1(a). The superconducting regions are realized by the superconducting proximity effect. The normal region is applied by a perpendicular electric field and irradiated by an off-resonant right-circularly polarized light. The perpendicular electric field is used to tune the band gap based on the buckled structure of silicene, while the off-resonant light can open a valley-dependent gap in terms of the Floquet theory [29,30]. This paper is organized as follows. In Sec. II, the model and basic formulas are constructed. In Secs. III and IV, the theoretical treatments and numerical results for the Andreev bound states and the Josephson effect are presented and discussed, respectively. Finally, in Sec. V, the conclusion of this work is given.

II. MODEL AND FORMALISM

In the considered system, the electron and hole excitations are described by the Dirac–Bogoliubov–de Gennes (DBdG)

---

[*]Author to whom correspondence should be addressed: gjin@nju.edu.cn
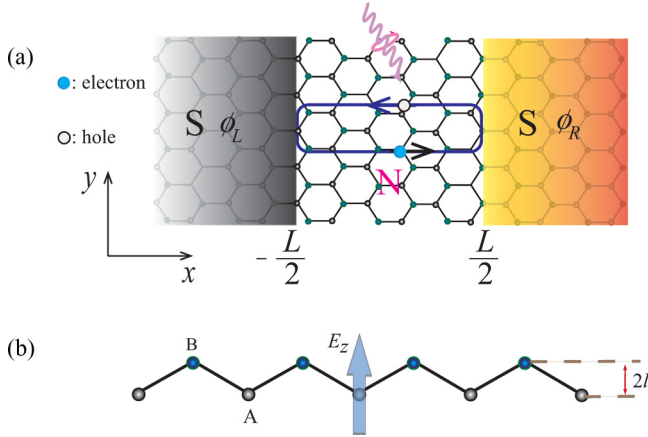
FIG. 1. Schematic diagrams for (a) the top view of a silicene-based Josephson junction and (b) the side view of silicene. An applied external electric field and an off-resonant right-circularly polarized light in the normal region are also shown.

equation [31]

$$
\begin{pmatrix} \mathcal{H} - E_F & \Delta(T) \\ \Delta^*(T) & E_F - \mathcal{T}\mathcal{H}\mathcal{T}^{-1} \end{pmatrix} \begin{pmatrix} u_e \\ v_h \end{pmatrix} = \varepsilon \begin{pmatrix} u_e \\ v_h \end{pmatrix}. \quad (1)
$$

Here ε is the excited energy relative to the Fermi level E_F, and u_e (v_h) is the electronlike (holelike) quasiparticle wave function. $\Delta(T) = 0$ in the normal region, while $\Delta(T) = \Delta_0 \tanh(1.74\sqrt{\frac{T_c}{T} - 1})e^{i\phi_{L(R)}}$ in the left (right) superconducting region. The latter is the temperature-dependent energy-gap function for an s-wave superconductor, with Δ_0 being the zero-temperature energy gap, T_c being the transition temperature, and $\phi_{L(R)}$ being the macroscopic phase in the left (right) superconductor. In the process of calculations, $k_B T_c = \frac{2\Delta_0}{3.53}$, with $\Delta_0 = 1$ meV, which is used as the energy unit.

The single-particle Hamiltonian is

$$
\mathcal{H} = \begin{pmatrix} \mathcal{H}_+ & 0 \\ 0 & \mathcal{H}_- \end{pmatrix}, \quad (2)
$$

in which

$$
\mathcal{H}_\eta = -i\hbar v_F(s_x \partial_x + \eta s_y \partial_y)\sigma_0 + \eta \lambda_{so} s_z \sigma_z \\ + (\eta F_\omega - l E_z)s_z \sigma_0 - U, \quad (3)
$$

where $\eta = \pm$ denote the two valleys of the band structure, $v_F = 5.5 \times 10^5$ m/s is the Fermi velocity, $s_{x,y,z}$ and σ_z are 2×2 Pauli matrices, σ_0 is the unit matrix, and the positive electrostatic potential U can be adjusted by doping or a gate voltage in the superconducting regions and is zero in the normal region. $\lambda_{so} = 3.9$ meV is the intrinsic spin-orbit coupling of silicene. $l = 0.23$ Å is the half distance between the two sublattice planes in which a perpendicular electric field E_z can be applied due to the buckled structure, as shown in Fig. 1(b). The illumination parameter is $F_\omega = \frac{e^2 E_0^2 v_F^2}{\hbar \omega^3}$, with E_0 being the amplitude of the electric field and ω being the frequency of the off-resonant right-circularly polarized light, as defined in the Floquet theory [29,30].

The time-reversal operator is expressed by $\mathcal{T} = i\eta_x \otimes s_z \otimes \sigma_y C$, with η_x being the Pauli matrix and C being the complex-conjugation operator. By substituting it into Eq. (1), Eq. (1)

can be decoupled into four sets of independent equations after matrix transformation, i.e.,

$$
\begin{pmatrix} \mathcal{H}_{\eta\sigma} + \eta F_\omega s_z - E_F & \Delta(T) \\ \Delta^*(T) & E_F - (\mathcal{H}_{\eta\sigma} - \eta F_\omega s_z) \end{pmatrix} \begin{pmatrix} u_e \\ v_h \end{pmatrix} = \varepsilon \begin{pmatrix} u_e \\ v_h \end{pmatrix}, \quad (4)
$$

where $\mathcal{H}_{\eta\sigma} = -i\hbar v_F(s_x \partial_x + \eta s_y \partial_y) + (\eta\sigma\lambda_{so} - lE_z)s_z - U$, with $\sigma = \pm 1$ being the spin index.

In the normal region, when ε and transverse momentum k_y are known, we obtain the four eigenstates by solving the DBdG equation and keeping the probability current conservation. They are

$$
\psi_{e,\eta\sigma}^\pm = \frac{e^{\pm ik_{xe}x + ik_y y}}{\sqrt{A\cos\theta}}(e^{\mp i\eta\theta/2}, \pm Ae^{\pm i\eta\theta/2}, 0, 0)^T,
$$

$$
\psi_{h,\eta\sigma}^\pm = \frac{e^{\pm ik_{xh}x + ik_y y}}{\sqrt{B\cos\varphi}}(0, 0, e^{\mp i\eta\varphi/2}, \mp Be^{\pm i\eta\varphi/2})^T. \quad (5)
$$

The state $\psi_{e,\eta\sigma}^+$ ($\psi_{h,\eta\sigma}^+$) denotes the electron (hole) moves in the $+x$ direction, while $\psi_{e,\eta\sigma}^-$ ($\psi_{h,\eta\sigma}^-$) denotes the electron (hole) moves in the $-x$ direction. The longitudinal wave vector of the electron k_{xe} (hole k_{xh}), the incident angle of the electron θ, the reflection angle of the corresponding hole φ, and the oscillation amplitudes A and B are all functions of the intrinsic and extrinsic quantities λ_{so}, E_z, F_ω, ε, and E_F and are calculated in the Appendix.

In the two superconducting regions, considering the heavily doped regime to ensure $E_F + U \gg \Delta(T)$, ε, and λ_{so}, the simplified wave functions are obtained as

$$
\psi_{SL}^\pm = e^{ik_{SL\pm}x + ik_y y}(e^{\mp i\beta}, \pm e^{\mp i\beta}, e^{-i\phi_L}, \pm e^{-i\phi_L})^T,
$$

$$
\psi_{SR}^\pm = e^{ik_{SR\pm}x + ik_y y}(e^{\mp i\beta}, \mp e^{\mp i\beta}, e^{-i\phi_R}, \mp e^{-i\phi_R})^T, \quad (6)
$$

where

$$
k_{SL(SR)\pm} = [-(+)i\Delta(T)\sin\beta \pm U]/\hbar v_F \quad (7)
$$

and

$$
\beta = \begin{cases} -i \operatorname{arcosh}[\varepsilon/\Delta(T)] & \varepsilon > \Delta(T), \\ \arccos[\varepsilon/\Delta(T)] & \varepsilon < \Delta(T). \end{cases} \quad (8)
$$

Referring to Eq. (6), the state $\psi_{SL(SR)}^+$ ($\psi_{SL(SR)}^-$) represents the wave function of a quasielectron (quasihole) for $\varepsilon > \Delta(T)$ or is the coherent superposition of the electron and hole excitations for $\varepsilon < \Delta(T)$.

For the Josephson effect considered here, which is similar to the short graphene-based SNS junction [17], the supercurrent across the junction between two superconductors is mainly carried by the bound states, known as the Andreev bound states (ABSs), which are the result of the closed-loop motion of the particles with discrete subgap energies, shown in Fig. 1(a). One can see that it is usually sufficient to find the ABSs for calculating the supercurrent carried by them. By summing over the energy $\varepsilon_{n\eta\sigma}$ of subgap quasiparticles at finite temperature T, the Josephson current J passing through the junction is given as

$$
J = -\frac{2e}{\hbar} \sum_{n\eta\sigma} \int N(\varepsilon_{n\eta\sigma}) \tanh\left(\frac{\varepsilon_{n\eta\sigma}}{2k_B T}\right) \frac{d\varepsilon_{n\eta\sigma}}{d\phi} \cos\theta d\theta, \quad (9)
$$

where n represents the number of ABSs, $N(\varepsilon_{n\eta\sigma}) = (W/\pi\hbar v_F)\sqrt{(\varepsilon_{n\eta\sigma} + E_F)^2 - (\eta\sigma\lambda_{so} - lE_z + \eta F_\omega)^2}$ are the transverse modes in a silicene monolayer of width W, and $\phi = \phi_R - \phi_L$ is the phase difference. The detailed process for calculating the ABSs is given in the Appendix.

III. ANDREEV BOUND STATES

The Andreev reflection and ABSs have been discussed for silicene-based superconducting junctions without off-resonant light [21]. The results in Ref. [21] can be reproduced by suppressing the light in the present case. According to the pairing rule referred to in Sec. I and the fact that the light-induced gap is always enlarged at one valley [8], the Andreev reflection is reduced with increasing F_ω. Here we focus on the light-modulated ABSs.

Before investigating the ABSs, the qualitative analysis, similar to the ferromagnetic Josephson junction [32,33], is instructive for further treatment in our model. From Eq. (3), the dispersion relation in the normal region is obtained as

$$E_{\eta\sigma} = \pm\sqrt{(\hbar v_F k)^2 + (\eta\sigma\lambda_{so} - lE_z + \eta F_\omega)^2}. \quad (10)$$

Considering the normal incidence, two paired electrons at the Fermi energy [32] will have the center-of-mass wave vector

$$q = k_x(\eta, \sigma) - k_x(-\eta, -\sigma), \quad (11)$$

where $k_x(\eta, \sigma) = \sqrt{E_F^2 - (\eta\sigma\lambda_{so} - lE_z + \eta F_\omega)^2}/\hbar v_F$ is derived from Eq. (10). We can see that the nonzero q can appear if $F_\omega \neq 0$. This is similar to the case in the ferromagnetic Josephson junction in which nonzero q is generated by the spin splitting. So the Josephson current reversal can be realized by irradiating an off-resonant light.

For the sake of revealing the influences of lE_z and F_ω on the ABSs and finding the essential relation between the ABS level and the Josephson current in Eq. (9), we still consider the normal incidence and derive from Eqs. (A8) and (A9) the Andreev bound level as

$$\frac{\varepsilon_{\eta\sigma}}{\Delta(T)} = \pm\frac{\sqrt{1 - \frac{X(Z-\cos\phi)\pm\sqrt{Y^2[X^2+Y^2-(Z-\cos\phi)^2]}}{X^2+Y^2}}}{\sqrt{2}} \quad (12)$$

and then the related velocity factor as

$$\frac{d\varepsilon_{\eta\sigma}}{\Delta(T)d\phi} = \pm\frac{f\sin\phi}{2\sqrt{2}\sqrt{1 - \frac{X(Z-\cos\phi)\pm\sqrt{Y^2[X^2+Y^2-(Z-\cos\phi)^2]}}{X^2+Y^2}}}, \quad (13)$$

where $f = (-X \pm \frac{Y(Z-\cos\phi)}{\sqrt{X^2+Y^2-(Z-\cos\phi)^2}})/(X^2 + Y^2)$. We can show in Fig. 2 the ϕ-dependent ABS level $\varepsilon_{n\eta\sigma}$ from Eq. (12). These ABSs are in the experimentally most favorable short-junction regime where length L of the normal region is small relative to the superconducting coherence length ξ, i.e., $L \ll \frac{\hbar v_F}{\Delta_0}$. Using reasonable values for the parameters here, it is confirmed that $L \ll 362$ nm. It should be pointed out that the nonzero incident angle does not affect the result of the qualitative analysis below. From calculations, one can confirm that each of these cases has eight ABS energy curves which cannot all be shown definitely in Figs. 2(a)–2(d) because of
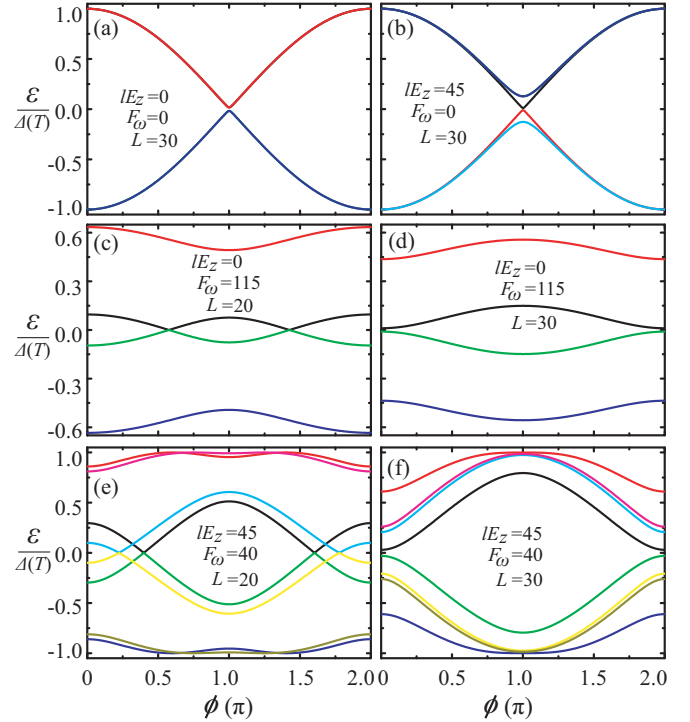
FIG. 2. (a)–(f) Andreev-bound-state level versus the phase difference with different lE_z, F_ω, and L. The Fermi energy $E_F = 120$, and the unit for the junction length is 1 nm.

the possible degeneracy of levels. From Figs. 2(a) to 2(f), the energy curves of the ϕ-dependent ABSs show entirely different tendencies with the varied electric field, off-resonant light, and junction length, which will obviously modulate the Josephson current.

In the absence of F_ω, corresponding to Figs. 2(a) and 2(b), $q = 0$, which leads to $Y = 0$ in Eq. (A9); then Eqs. (12) and (13) become the following formulas:

$$\frac{\varepsilon_{\eta\sigma}}{\Delta(T)} = \pm\sqrt{\frac{\frac{\cos\phi-Z}{X}+1}{2}} \quad (14)$$

and

$$\frac{d\varepsilon_{\eta\sigma}}{\Delta(T)d\phi} = \pm\frac{-\sin\phi}{2\sqrt{2}\sqrt{\frac{\cos\phi-Z}{X}+1}}. \quad (15)$$

We observe Eq. (9) and find that the direction of the Josephson current is dependent on the product of signs of the negative Andreev bound level $-\varepsilon_{n\eta\sigma}$ and its slope $\frac{d\varepsilon_{n\eta\sigma}}{d\phi}$. It is easy to judge that the sign of the Josephson current is always positive (negative) for $\phi \in [0,\pi)$ ($\phi \in [\pi,2\pi)$) from the above formulas. The same result can be obtained in Figs. 2(a) and 2(b), in which the product of the signs of an Andreev bound level and its slope are negative (positive) for $\phi \in [0,\pi)$ ($\phi \in [\pi,2\pi)$); then the value of the Josephson current remains positive (negative) for $\phi \in [0,\pi)$ ($\phi \in [\pi,2\pi)$). Whatever the junction length or electric field is, Figs. 2(a) and 2(b) always keep the same relation of ϕ-dependent ABSs due to time-reversal symmetry. These ABS-transferred Josephson currents
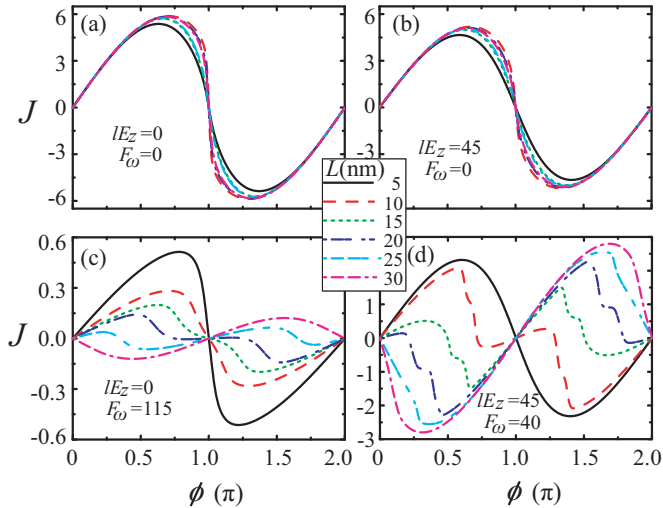
FIG. 3. (a)–(d) Josephson current versus the phase difference with different perpendicular electric fields, off-resonant lights, and junction lengths but fixed Fermi level $E_F = 120$.

FIG. 4. (a)–(d) the critical Josephson current versus the junction length with different perpendicular electric fields and off-resonant lights in the case of $E_F = 120$.

are the same as the traditional ones and are shown in Figs. 3(a) and 3(b).

In the presence of F_ω, besides the similar relation of ϕ-dependent ABS levels in Figs. 2(a) and 2(b), there exist two different relations of ϕ-dependent ABS levels shown in Figs. 2(c) and 2(d). They come from the fact that the combination of F_ω and λ_{so} leads to a nonzero center-of-mass wave vector of a Cooper pair, shown in Eq. (11). The slope of a ϕ-dependent ABS level is described by Eq. (13). The sign of the slope is determined by the F_ω-dependent function f, which will lead to the Josephson current reversal by adjusting F_ω. It is found that in Fig. 2(c), some products of the signs of the ABS levels and their slopes are negative, while some of their products are positive for $\phi \in [0,\pi)$, which will lead to the sign reversal at ϕ between 0 and π. Unfortunately, in this case, it is not easy to judge whether the 0-π transition occurs or not because the critical current cannot be estimated correctly. In contrast, in Fig. 2(d), the products of the signs of the ABS levels and their slope are opposite to the case in Figs. 2(a) and 2(b), which means the generation of the 0-π transition. Interestingly, in the presence of F_ω and lE_z, shown in Figs. 2(e) and 2(f), although the relations of the ϕ-dependent ABS levels are the same as in Figs. 2(c) and 2(d), there exists another origin of nonzero q, i.e., the valley polarization-induced nonzero q. All these analyses are confirmed in Figs. 3(c) and 3(d), respectively.

From the numerical calculations and analyses above, it is found that the property of the Josephson current is dependent on the slope of a ϕ-dependent positive ABS level for $\phi \in [0,\pi]$ and the slope can be three different types, i.e., the negative slope, the positive slope, and the hybrid of negative and positive slopes. The negative (positive) slope is the sign of the 0 (π) state, while the hybrid of negative and positive slopes cannot give a qualitative result. Further, when the effect of temperature is taken into account, the distribution function of ABSs, that is, $\tanh(\frac{\varepsilon_{n\eta\sigma}}{2k_BT})$, will affect the Josephson current. From Fig. 2, for the negative (positive) slope at $\phi \in [0,\pi]$, no matter how the temperature is adjusted, the
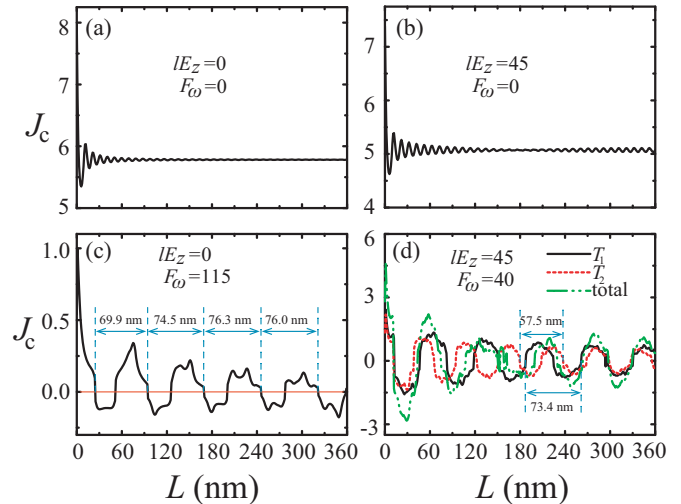
Josephson current always shows the 0 (π) state. However, for the hybrid of negative and positive slopes at $\phi \in [0,\pi]$, there is a competition between the ABSs for generating the Josephson current. The temperature-dependent distribution function of ABSs will affect the competitive effect and may lead to the temperature-induced Josephson current reversal at some phase differences. But in our model, this current reversal is not the 0-π transition, which can be confirmed by numerical calculations in Fig. 5 below.

IV. SUPERCURRENT REVERSAL

In terms of Eqs. (9) and (12)–(15), we have calculated the phase-difference-dependent Josephson current with different lE_z, F_ω, and junction length L at zero temperature, as shown in Fig. 3. The unit for Josephson current is $J_0 = \frac{2e}{\hbar}\frac{WE_F}{\pi\hbar v_F}$, and the Fermi energy is chosen at $E_F = 120$ meV. In Figs. 3(a) and 3(b), the Josephson current always shows the zero state with different junction lengths in pristine silicene and gated silicene, respectively. In the presence of off-resonant light or the coexistence of off-resonant light and the electric field, the 0-π transition is generated, as shown in Figs. 3(c) and 3(d). These numerical results are consistent with the preceding qualitative analysis.

In order to exhibit the characteristics of the junction-length-dependent Josephson current explicitly, the critical Josephson current J_c, with the same parameters as in Fig. 3, versus the junction length is plotted in Fig. 4. It is easy to find that J_c keeps the positive value in pristine or gated silicene, shown in Figs. 4(a) and 4(b), while it oscillates from the positive value to the negative value with increasing junction length in the presence of an off-resonant light, shown in Figs. 4(c) and 4(d). According to the phenomenological theory in the traditional ferromagnetic Josephson junction [32,33], one find that $J_c \propto \cos(|q|L)$, and its oscillation period is $2\pi/|q|$, which is ≈ 77.6 nm using Eq. (11), in approximate agreement with the numerical calculations from Eq. (9) in Fig. 4(c). In the coexistence of an electric field and an
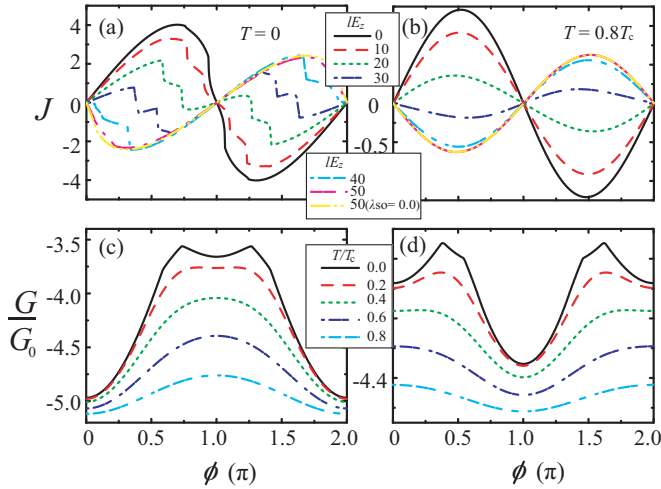
FIG. 5. (a) and (b) Josephson current versus the phase difference with different perpendicular electric fields at zero and nonzero temperatures, respectively. Also a comparison is made for Josephson current between the nonzero and zero spin-orbit couplings with $lE_z = 50$. Free-energy-phase relation at different temperatures for (c) $lE_z = 20$ and (d) $lE_z = 30$. The other parameters are $E_F = 120$, $F_\omega = 50$, $G_0 = \frac{WE_F}{\pi \hbar v_F} \Delta_0$, and $L = 20$ nm.

off-resonant light, shown in Fig. 4(d), there are two different nonzero $|q|$ from Eq. (11), i.e., $q_1 = |k_x(1,1) - k_x(-1,-1)|$ and $q_2 = |k_x(1,-1) - k_x(-1,1)|$. The oscillation periods of J_c are $T_1 \approx 71.6$ nm and $T_2 \approx 57.8$ nm, respectively, which agree with the numerical ones in Fig. 4(d). These two different oscillation periods make the total critical current chaotic, shown in Fig. 4(d) by the green dot-dashed line. Although the junction length cannot be changed continuously in measurements, Fig. 4 provides a reference for choosing a suitable junction length in experiment.

Although it is not a handleable way to realize the 0-π transition by changing the junction length, the control of the perpendicular electric field and off-resonant light is feasible in experiment. In Fig. 5(a), curves of the Josephson current versus the phase difference are plotted with different electric fields and a fixed off-resonant light $F_\omega = 50$. The phenomenon of the 0-π transition is clearly shown. We observe the Josephson current in Fig. 5(a) carefully and find that the sign of the Josephson current is reversed at ϕ between 0 and π when $lE_z = 20$ (or 30). This is different from the case of $lE_z = 10$ (or 40 or 50) in which the change of sign only occurs at $\phi = \pi$. The reason is that the hybrid of negative and positive slopes of ϕ-dependent ABS levels leads to the current reversal at $\phi \in [0,\pi)$, which was discussed in Sec. III. It should be emphasized that, in Fig. 5(a), this 0-π transition originating from the valley polarization is different from the traditional one where the spin splitting plays the key role. We neglect the spin-orbit coupling λ_{so} when $lE_z \gg \lambda_{so}$ (the yellow double-dot-dashed line) and find that this approximate result is almost in agreement with the accurate calculation (the magenta dot-dashed line). Therefore, we confirm that the valley degree of freedom in a silicene-based SNS junction plays the same role as the spin degree of freedom in an SFS junction in the 0-π transition.

The above numerical calculations are performed at zero temperature. In actual experiments, the effect of temperature on Josephson current needs to be considered. When all the slopes of ϕ-dependent ABS levels are negative (positive) at $\phi \in (0,\pi)$, it is obvious that temperature only affects the magnitude of the Josephson current, while the Josephson current reversal cannot be generated. Here we focus on the discussion of the hybrid of negative and positive slopes of ϕ-dependent ABS levels. In Fig. 5(b) with $lE_z = 20(30)$ and $F_\omega = 50$, the Josephson current reversal occurs at some ϕ at a finite temperature. This temperature-induced Josephson current reversal is attributed to the temperature-modulated competitive effect between the ABS levels, which was illuminated in Sec. III explicitly. However, the critical current is not reversed, which means that the temperature-induced Josephson current reversal is not the 0-π transition. We can show the 0 or π state by observing the free energy [34]

$$G = -k_B T \sum_{n\eta\sigma} \int N(\varepsilon_{n\eta\sigma}) \ln \left[2\cosh\left(\frac{\varepsilon_{n\eta\sigma}}{2k_B T}\right) \right] \cos\theta d\theta,$$

(16)

shown in Figs. 5(c) and 5(d). The minimum values of free energy are unchanged with increasing temperature, which means that the 0 or π state is not affected by the environmental temperature.

It is necessary to discuss the parameter selection. The junction length was analyzed in Sec. III. In the presence of F_ω ($lE_z = 0$), by checking Eq. (11), the nonzero center-of-mass wave vector $|q| \to 0$ when $E_F \gg F_\omega, \lambda_{so}$, and the maximum $|q|_{max} = 2\sqrt{\lambda_{so} F_\omega}/\hbar v_F$ when $E_F = \lambda_{so} + F_\omega$. The larger the nonzero wave vector is, the smaller the oscillation period becomes. If we choose $F_\omega = 2\lambda_{so}$, which is the same as in Ref. [8], the oscillation period is about 205 nm. Although the parameters are allowed in theory, they may not be able to meet the requirement of being short junction in experiment. In order to exhibit the parameter dependence explicitly, the contour plot for J_c versus F_ω and E_F with $L = 30$ nm, which is in the experimentally most relevant short-junction regime, is shown in Fig. 6(a). The dark blue region is the π state. In the coexistence of F_ω and E_z, in principle, it is difficult to provide a qualitative analysis due to the two different nonzero wave vectors q_1 and q_2. But we can neglect the spin-orbit coupling λ_{so} when $lE_z \gg \lambda_{so}$, which lets us obtain the maximum nonzero center-of-mass wave vector $|q|_{max} = 2\sqrt{lE_z F_\omega}/\hbar v_F$ when $E_F = lE_z + F_\omega$. The contour plot for J_c versus lE_z and F_ω can also be plotted, as shown in Fig. 6(b). We can use this simple relation combined with Figs. 6(a) and 6(b) to estimate the values of parameters allowed in experiment. In fact, the values of lE_z, F_ω, and E_F in Figs. 2–5 are available in experiment. In theory, in order to compare with Ref. [8], we artificially set $L = 100$ nm, and the values of lE_z and F_ω are the same as those in Ref. [8], shown in Fig. 6(c). Unfortunately, J_c cannot be used to distinguish the different topological phases displayed in Ref. [8] because J_c depends on the nonzero wave vector and junction length. Excitingly, the combination of F_ω and λ_{so} can generate the 0-π transition when we compare Fig. 6(c) with Fig. 6(d), in which λ_{so} is neglected artificially. This is a particular property of silicene which cannot be found in graphene due to the very weak spin-orbit coupling. We give
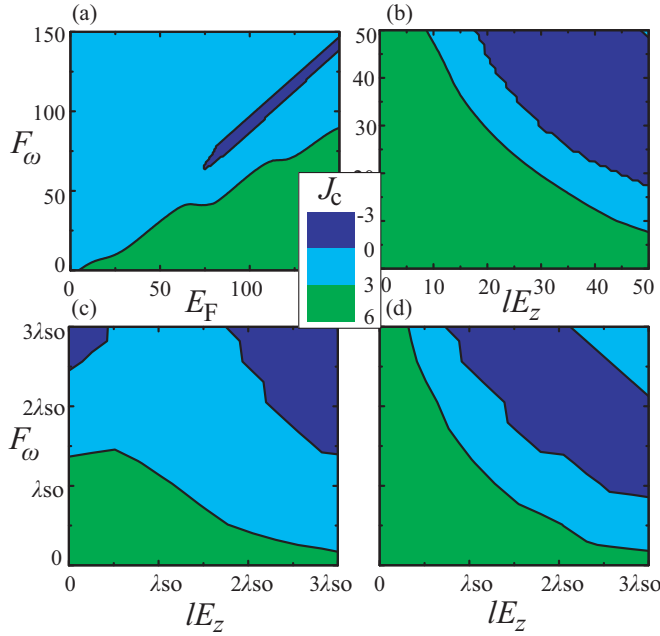
FIG. 6. The contour plot for critical current J_c versus (a) E_F and F_ω with $L = 30$ nm and $lE_z = 0$, (b) lE_z and F_ω with $L = 30$ nm and $E_F = 120$, and (c) and (d) lE_z and F_ω with $L = 100$ nm, $E_F = 20$, and $\lambda_{so} = 3.9$ and 0, respectively.

a detailed comparison between silicene and graphene in the following.

Although the 0-π transition can be generated in the irradiated graphene-based SNS junction with a staggered sublattice potential, there are three weaknesses. First, compared with the gate-tunable gap in silicene, the gap induced by the staggered sublattice potential in graphene is not flexibly controlled in experiment. Second, when only the off-resonant light is irradiated in the graphene-based Josephson junction, the 0-π transition cannot be generated for small q due to the very weak spin-orbit interaction. This is different from the irradiated silicene in which the 0-π transition can be realized, shown in Fig. 3(c). Third, there is a requirement for the off-resonant light that its photon energy must be larger than the bandwidth of graphene (silicene), i.e., $\hbar\omega \gg \gamma$, where $\gamma = 2.82(1.6)$ eV is the nearest-neighbor hopping energy for graphene (silicene). This means that the frequency for graphene (silicene) is about 3500 (1000) THz [8,30]. From these three aspects, we can see that the realization of the 0-π transition in silicene has more advantages than in graphene.

V. CONCLUSIONS

In summary, we have studied the Andreev bound states and Josephson effect in a silicene-based SNS junction gated by an electric field and irradiated by an off-resonant light. Three kinds of slopes of the ϕ-dependent ABS levels for $\phi \in [0,\pi]$, i.e., the negative slope, the positive slope, and the hybrid of negative and positive slopes, were found. The negative (positive) slope determines the positive (negative) Josephson current, i.e., the 0 (π) state, while the state of the Josephson junction cannot be judged from the hybrid of

negative and positive slopes due to the ambiguous critical current.

The pristine- or gated-silicene-based Josephson junction, in which the phase-difference-dependent ABSs always show a negative slope, cannot realize the 0-π transition because of the time-reversal symmetry. In contrast, owing to the combination of the intrinsic spin-orbit coupling and the broken time-reversal symmetry induced by an off-resonant light, the 0-π transition is generated by the ABSs with the positive slope.

It should be emphasized that the 0-π transition here is tuned by a perpendicular electric field, and an off-resonant light from the latter valley polarization is produced uniquely. The valley degree of freedom in the present silicene-based SNS junction, which is analogous to the spin degree of freedom in the conventional SFS junctions, plays a key role in the realization of the 0-π transition. It is not very difficult technically to verify these results experimentally. Our finding provides an alternative mechanism and a new operating method for realizing the 0-π transition.

APPENDIX: SOME DETAILS ABOUT SOLVING THE ANDREEV BOUND STATES

In the normal region shown in Fig. 1(a), there are two interfaces, one at $x = -L/2$ separating the left superconductor with phase $\phi_L = -\phi/2$ and the other at $x = L/2$ separating the right superconductor with phase $\phi_R = \phi/2$. The parameters in Eq. (5) are given by the definitions

$$
\begin{aligned}
A_\pm &= \sqrt{(E_F + \varepsilon) \pm (\eta\sigma\lambda_{so} - lE_z + \eta F_\omega)}/\sqrt{\hbar v_F}, \\
B_\pm &= \sqrt{(E_F - \varepsilon) \pm (\eta\sigma\lambda_{so} - lE_z - \eta F_\omega)}/\sqrt{\hbar v_F}, \\
k_{xe} &= A_+ A_- \cos\theta, \quad k_{xh} = g B_+ B_- \cos\varphi, \\
g &= \text{sgn}[(\varepsilon - E_F) - |\,\eta\sigma\lambda_{so} - lE_z - \eta F_\omega\,|], \\
\theta &= \arcsin[k_y/(A_+ A_-)], \quad \varphi = g\arcsin[k_y/(B_+ B_-)], \\
A &= A_-/A_+, \quad B = B_+/B_-.
\end{aligned} \tag{A1}
$$

It is noted that the Andreev reflection is specular for $g = 1$ and is retroreflected for $g = -1$. There will be no Andreev reflection if the incident angle is beyond the critical angle

$$
\theta_c = \arcsin\frac{B_+ B_-}{A_+ A_-}. \tag{A2}
$$

According to Eq. (6), the boundary conditions at the two interfaces are given by

$$
v_h(-L/2) = \mathcal{U} u_e(-L/2), \quad v_h(L/2) = \mathcal{U}^{-1} u_e(L/2), \tag{A3}
$$

with

$$
\mathcal{U} = \begin{pmatrix} \cos\beta & i\sin\beta \\ i\sin\beta & \cos\beta \end{pmatrix} e^{i\phi/2}. \tag{A4}
$$

The states of the left and right interfaces are related as

$$u_e(L/2) = \mathcal{M}_e u_e(-L/2), \quad v_h(L/2) = \mathcal{M}_h v_h(-L/2),$$

$$\text{(A5)}$$

where the transfer matrices are

$$\mathcal{M}_e = \frac{1}{\cos\theta}\begin{pmatrix} \cos(k_{xe}L - \eta\theta) & i\sin(k_{xe}L)/A \\ iA\sin(k_{xe}L) & \cos(k_{xe}L + \eta\theta) \end{pmatrix},$$

$$\mathcal{M}_h = \frac{1}{\cos\varphi}\begin{pmatrix} \cos(k_{xh}L - \eta\varphi) & -i\sin(k_{xh}L)/B \\ -iB\sin(k_{xh}L) & \cos(k_{xh}L + \eta\varphi) \end{pmatrix}. \quad \text{(A6)}$$

For the existence of an Andreev bound state in the Josephson junction, the transfer matrix for the round trip from $x = -\frac{L}{2}$ to $x = \frac{L}{2}$ and then back to $x = -\frac{L}{2}$ is unimodular, i.e.,

$$u_e(-L/2) = \mathcal{X} u_e(-L/2),$$
$$\det \mathcal{X} = \det\left[\mathcal{M}_e^{-1}\mathcal{U}\mathcal{M}_h\mathcal{U}\right] = 1. \quad \text{(A7)}$$

Solving Eq. (A7), we obtain

$$\cos\phi = X\cos 2\beta + Y\sin 2\beta + Z, \quad \text{(A8)}$$

where

$$X = \cos(k_{xe}L)\cos(k_{xh}L)$$
$$- \frac{(1+A^2)(1+B^2)}{4AB}\frac{\sin(k_{xe}L)\sin(k_{xh}L)}{\cos\theta\cos\varphi},$$

$$Y = \frac{1+B^2}{2B}\frac{\cos(k_{xe}L)\sin(k_{xh}L)}{\cos\varphi}$$
$$+ \frac{1+A^2}{2A}\frac{\sin(k_{xe}L)\cos(k_{xh}L)}{\cos\theta},$$

$$Z = \frac{(1-A^2)(1-B^2)\sin(k_{xe}L)\sin(k_{xh}L)}{4AB\cos\theta\cos\varphi}$$
$$- \sin(k_{xe}L)\sin(k_{xh}L)\tan\theta\tan\varphi. \quad \text{(A9)}$$

When $\lambda_{\mathrm{so}} = lE_z = F_\omega = 0$, then $A = B = 1$. This reproduces the results for graphene in Ref. [17].

It is reasonable to analyze the Josephson effect in the experimentally most relevant short-junction regime where the length L of the normal region is smaller than the superconducting coherence length ξ, i.e., $L \ll \frac{\hbar v_{\mathrm{F}}}{\Delta_0}$. So the junction length satisfies $L \ll 362$ nm. Considering $E_{\mathrm{F}} \gg \varepsilon$, then $X \approx X(\varepsilon = 0)$, $Y \approx Y(\varepsilon = 0)$, and $Z \approx Z(\varepsilon = 0)$. Thus, substituting Eq. (A9) into Eq. (A8), we can derive Eq. (12) and its derivative, Eq. (13).

[1] G. G. Guzmán-Verri and L. C. Lew Yan Voon, Phys. Rev. B **76**, 075131 (2007).

[2] S. Cahangirov, M. Topsakal, E. Aktürk, H. Şahin, and S. Ciraci, Phys. Rev. Lett. **102**, 236804 (2009).

[3] N. D. Drummond, V. Zólyomi, and V. I. Fal'ko, Phys. Rev. B **85**, 075423 (2012).

[4] P. Vogt, P. De Padova, C. Quaresima, J. Avila, E. Frantzeskakis, M. C. Asensio, A. Resta, B. Ealet, and G. Le Lay, Phys. Rev. Lett. **108**, 155501 (2012).

[5] A. Fleurence, R. Friedlein, T. Ozaki, H. Kawai, Y. Wang, and Y. Yamada-Takamura, Phys. Rev. Lett. **108**, 245501 (2012).

[6] C.-C. Liu, W. Feng, and Y. Yao, Phys. Rev. Lett. **107**, 076802 (2011).

[7] M. Ezawa, Phys. Rev. Lett. **109**, 055502 (2012).

[8] M. Ezawa, Phys. Rev. Lett. **110**, 026603 (2013).

[9] T. Yokoyama, Phys. Rev. B **87**, 241409(R) (2013).

[10] K. Zberecki, M. Wierzbicki, J. Barnaś, and R. Swirkowicz, Phys. Rev. B **88**, 115404 (2013).

[11] Kh. Shakouri, P. Vasilopoulos, V. Vargiamidis, and F. M. Peeters, Phys. Rev. B **90**, 125444 (2014).

[12] Z.-X. Guo, Y.-Y. Zhang, H. Xiang, X.-G. Gong, and A. Oshiyama, Phys. Rev. B **92**, 201413(R) (2015).

[13] M. Ezawa, Phys. Rev. B **87**, 155415 (2013).

[14] Z. P. Niu and S. Dong, Appl. Phys. Lett. **104**, 202401 (2014).

[15] Y. Xu, X. Zhou, and G. Jin, Appl. Phys. Lett. **108**, 203104 (2016).

[16] C. W. J. Beenakker, Phys. Rev. Lett. **97**, 067007 (2006).

[17] M. Titov and C. W. J. Beenakker, Phys. Rev. B **74**, 041401(R) (2006).

[18] J. Linder, T. Yokoyama, D. Huertas-Hernando, and A. Sudbø, Phys. Rev. Lett. **100**, 187004 (2008).

[19] C. W. J. Beenakker, Rev. Mod. Phys. **80**, 1337 (2008).

[20] X. Zhai and G. Jin, Phys. Rev. B **89**, 085430 (2014).

[21] J. Linder and T. Yokoyama, Phys. Rev. B **89**, 020504(R) (2014).

[22] B. D. Josephson, Rev. Mod. Phys. **46**, 251 (1974).

[23] A. F. Andreev, Sov. Phys. JETP **19**, 1228 (1964).

[24] I. O. Kulik, Sov. Phys. JETP **30**, 944 (1970).

[25] V. V. Ryazanov, V. A. Oboznov, A. Yu. Rusanov, A. V. Veretennikov, A. A. Golubov, and J. Aarts, Phys. Rev. Lett. **86**, 2427 (2001).

[26] A. I. Buzdin, L. N. Bulaevskii, and S. V. Panyukov, Pis'ma Zh. Eksp. Teor. Fiz. **35**, 147 (1982) [JETP Lett. **35**, 178 (1982)].

[27] A. I. Buzdin, Rev. Mod. Phys. **77**, 935 (2005).

[28] F. Qi and G. Jin, J. Appl. Phys. **115**, 173701 (2014).

[29] T. Kitagawa, T. Oka, A. Brataas, L. Fu, and E. Demler, Phys. Rev. B **84**, 235108 (2011).

[30] X. Zhou, Y. Xu, and G. Jin, Phys. Rev. B **92**, 235436 (2015).

[31] P. G. de Gennes, *Superconductivity of Metals and Alloys* (Benjamin, New York, 1966).

[32] E. A. Demler, G. B. Arnold, and M. R. Beasley, Phys. Rev. B **55**, 15174 (1997).

[33] F. S. Bergeret, A. F. Volkov, and K. B. Efetov, Rev. Mod. Phys. **77**, 1321 (2005).

[34] G. Annunziata, H. Enoksen, J. Linder, M. Cuoco, C. Noce, and A. Sudbø, Phys. Rev. B **83**, 144520 (2011).